DOI: 10.6060/ivkkt.20266908.7185

ВЗАИМОСВЯЗЬ МЕЖДУ ОБРАБОТКОЙ, МИКРОСТРУКТУРОЙ И ДИЭЛЕКТРИЧЕСКИМИ СВОЙСТВАМИ В ТВЕРДОТЕЛЬНЫХ СПЕЧЕННЫХ КЕРАМИЧЕСКИХ КОМПОЗИТАХ Al–CaB_6

Эман А. Мвафи, Гехан Т. Эль-Бассиуни, Сайед Х. Кенави, Эсмат М.А. Хамзави

Эман А. Мвафи (ORCID 0000-0002-7638-1343)

Кафедра физической химии, Национальный исследовательский центр, Институт передовых материалов, технологий и минеральных ресурсов, ул. Эль-Бухут, 33, Докки, Каир, 12622, Египет

Гехан Т. Эль-Бассиуни (ORCID 0000-0001-8438-0570), Саид Х. Кенави (ORCID 0000-0003-0850-9496)*

Кафедра огнеупоров, керамики и строительных материалов, Национальный исследовательский центр, ул. Эль-Бухут, Докки - 12622, Гиза, Египет
E-mail: ksayed6631@gmail.com*

Эсмат М.А. Хамзави (ORCID0000-0002-0984-9911)

Отдел исследований стекла, Национальный исследовательский центр, Институт передовых материалов, технологий и минеральных ресурсов, ул. Э. Бухут, 33, Докки, Каир, 12622, Египет

В данном исследовании систематически изучаются корреляции между условиями обработки, микроструктурой и диэлектрическими свойствами композитов из гексаборида алюминия и кальция (Al–CaB_6), полученных методом твердофазного спекания. Композиты с различным содержанием CaB_6 (10–50 мас.%) были спечены, что привело к образованию мелкозернистой микроструктуры. Было подтверждено сохранение критически важных октаэдрических единиц B_6 в CaB_6, а также образование корунда и других оксидных фаз. Ключевым выводом является то, что увеличение содержания CaB_6 значительно улучшает диэлектрические характеристики, о чем свидетельствует более высокая диэлектрическая постоянная и проводимость на переменном токе, а также снижение потерь энергии на высоких частотах. Это улучшение объясняется двумя микроструктурными факторами: (1) усилением межфазной поляризации на границах фаз и (2) образованием перколяционных сетей, облегчающих перенос заряда. Поведение при уплотнении в значительной степени определяется балансом между содержанием металлического Al и температурой спекания. Композиция 80 мас.% Al – 20 мас.% CaB_6, спеченная при 1200 °C, обеспечивает наиболее благоприятную микроструктурную консолидацию с минимальной пористостью. Падение плотности при 1100 °C отмечает промежуточную стадию, на которой взаимодействие между диффузией и образованием жидкой фазы становится нестабильным, что приводит к снижению эффективности уплотнения. Электрический отклик демонстрирует распределенное релаксационное поведение, указывающее на сложную микроструктуру межфазной границы. Эти специально подобранные свойства делают композиты Al–CaB_6 перспективными материалами для современных высокочастотных компонентов и конденсаторов следующего поколения.

Ключевые слова: гексаборид алюминия и кальция, керамические композиты, диэлектрические свойства, твердотельное спекание, релаксационная динамика, межфазная поляризация

Для цитирования:

Эман А. Мвафи, Гехан Т. Эль-Бассиуни, Сайед Х. Кенави, Эсмат М.А. Хамзави Взаимосвязь между обработкой, микроструктурой и диэлектрическими свойствами в твердотельных спеченных керамических композитах Al–CaB_6. *Изв. вузов. Химия и хим. технология*. 2026. Т. 69. Вып. 8. С. 12–24. DOI: 10.6060/ivkkt.20266908.7185.

For citation:

Eman A. Mwafy, Gehan T. El-Bassyouni, Sayed H. Kenawy, Esmat M.A. Hamzawy Processing–microstructure–dielectric property correlations in solid-state sintered Al–CaB_6 ceramic composites. *ChemChemTech* [*Izv. Vyssh. Uchebn. Zaved. Khim. Khim. Tekhnol.*]. 2026. V. 69. N 8. P. 12–24. DOI: 10.6060/ivkkt.20266908.7185.

PROCESSING–MICROSTRUCTURE–DIELECTRIC PROPERTY CORRELATIONS IN SOLID-STATE SINTERED Al–CaB_6 CERAMIC COMPOSITES

Eman A. Mwafy, Gehan T. El-Bassyouni, Sayed H. Kenawy, Esmat M.A. Hamzawy

Eman A. Mwafy (ORCID 0000-0002-7638-1343)

Physical Chemistry Dept., National Research Centre, Advanced Materials Technology and Mineral Resources Research Institute, 33 El‑Buhouth St., Dokki, Cairo, 12622, Egypt

Gehan T. El-Bassyouni (ORCID 0000-0001-8438-0570), Sayed H. Kenawy (ORCID 0000-0003-0850-9496)*

Refractories, Ceramics and Building Materials Department, National Research Centre, El Buhouth St., Dokki - 12622, Giza, Egypt
Email: ksayed6631@gmail.com*

Esmat M.A. Hamzawy (ORCID0000-0002-0984-9911)

Glass Research Department, National Research Centre, Advanced Materials Technology and Mineral Resources Research Institute, 33 El‑Buhouth St., Dokki, Cairo, 12622, Egypt

This study systematically investigates the correlations between processing conditions, microstructure, and dielectric properties of aluminum–calcium hexaboride (Al–CaB_6) composites fabricated via solid-state sintering. Composites with varying CaB_6 content (10–50 wt.%) were sintered, resulting in a fine-grained microstructure. The preservation of critical B_6 octahedral units within CaB_6 was confirmed, alongside the formation of corundum and other oxide phases. A key finding is that increasing CaB_6 content significantly enhances dielectric performance, evidenced by a higher dielectric constant and AC conductivity, coupled with reduced energy loss at high frequencies. This improvement is attributed to two microstructural factors: (1) intensified interfacial polarization at phase boundaries, and (2) the formation of percolation networks that facilitate charge transport. Densification behavior is strongly governed by the balance between metallic Al content and sintering temperature. The 80 wt.% Al–20 wt.% CaB_6 composition sintered at 1200 °C provides the most favorable microstructural consolidation with minimal porosity. A density dip at 1100 °C marks an intermediate stage where the interplay between diffusion and liquid-phase formation is unstable, leading to reduced compaction efficiency. The electrical response exhibits distributed relaxation behavior, indicative of a complex interfacial microstructure. These tailored properties position Al–CaB_6 composites as promising materials for advanced high-frequency components and next-generation capacitors.

Keywords: aluminum-calcium hexaboride, ceramic composites, dielectric properties, solid-state sintering, relaxation dynamics, interfacial polarization

INTRODUCTION

Ceramic materials are the cornerstone of modern industry, prized for their exceptional mechanical strength, chemical inertness, and resilience in high-temperature environments. Within this broad class of materials, aluminum–calcium hexaboride (Al–CaB_6) composites have emerged as a particularly promising candidate for extreme-service applications in aerospace and advanced engineering. This is due to their unique combination of exceptional hardness, remarkable thermal stability, and an excellent strength-to-weight ratio [1, 2].

The synergy between the metallic aluminum (Al) and the refractory ceramic calcium hexaboride (CaB_6) results in a composite that integrates the beneficial properties of both constituents. However, the ultimate performance of such a composite is not solely dictated by its chemical composition, but critically by its internal architecture and its microstructure. This microstructure is a direct consequence of the processing route employed. Among various synthesis techniques, the solid-state reaction method is a widely used and effective approach for fabricating these composites. This process involves the homogenization, compaction, and high-temperature sintering of precursor powders typically aluminum oxide (Al_2O_3), calcium oxide (CaO), and boron oxide (B_2O_3). While this method is established, a detailed understanding of how the processing parameters and the resulting microstructure ultimately

govern the functional properties, such as dielectric behavior, remains crucial for tailoring these materials for next-generation applications. It is this critical link between processing, microstructure, and functional dielectric properties that this investigation seeks to establish [3]. The general reaction can be expressed by *Karadimas and Salonitis*, 2023 [4] as:

$$2CaO + Al_2O_3 + 6B_2O_3 \rightarrow 2AlCaB_6 + 9O_2 \quad (1)$$

The solid-state reaction method is highly valued for producing Al–CaB_6 composites with precise stoichiometry and uniform microstructure (equation 1), making it a reliable choice for many industrial applications [5]. However, to achieve even greater control over the material's architecture, researchers employ advanced synthesis techniques. Chemical Vapor Deposition (CVD), for instance, uses gaseous precursors like $AlCl_3$, CaC_2, and B_2H_6 to deposit dense, high-purity Al–CaB_6 layers directly onto a substrate [6, 7]. This method is ideal for creating exceptionally pure and homogeneous coatings. In contrast, the sol-gel method operates at significantly lower temperatures. It begins with a liquid solution of metal alkoxides or nitrates, which undergoes hydrolysis and condensation to form a homogeneous gel. This gel is then dried and sintered to produce the final, dense ceramic. The key advantage of sol-gel is its ability to achieve exceptional compositional uniformity at a molecular level, prior to sintering [8].

The exceptional mechanical strength and thermal stability of aluminum–calcium hexaboride (Al–CaB_6) ceramics have established them as critical materials for demanding applications in aerospace, wear-resistant coatings, and high-temperature industrial systems [9]. This robustness is largely due to the strong interfacial bonding between the aluminum matrix and the CaB_6 reinforcement, which is critical for optimal mechanical performance [10]. Beyond their structural properties, Al–CaB_6 composites are of significant scientific and technological interest due to their tunable dielectric behavior. This tunability originates from the intrinsic nature of its constituents: the composite combines conductive aluminum with insulating CaB_6. The resulting heterogeneous microstructure, rich in internal interfaces and oxide layers, becomes the primary site for controlling charge transport and polarization mechanisms [11]. Consequently, the potential of these composites for next-generation capacitors, high-frequency electronics, and extreme-condition insulation hinges on our ability to engineer their dielectric performance. The key to this engineering lies at the interface between the chemically stable CaB_6 and the toughening, conductive aluminum. It is this interface that governs critical phenomena like polarization and energy storage [12]. Therefore, by deliberately tailoring the composite's microstructure, through variations in composition; it is possible to enhance interfacial polarization, control relaxation behavior, and minimize detrimental dielectric losses [13].

To systematically explore this structure-property relationship, the present study focuses on synthesizing Al–CaB_6 composites via the solid-state route with varying CaB_6 content. The fabricated composites were thoroughly characterized using XRD, SEM, and FTIR to correlate their structural and morphological evolution with their dielectric properties, as measured by electrical impedance spectroscopy. This work aims to provide a clear blueprint for tailoring Al–CaB_6 composites for specific electronic applications.

EXPERIMENTAL

Raw Materials and Sample Preparation

High-purity aluminum metal powder (98%, LOP-CHEM, India) and calcium hexaboride (CaB_6) powder (Elektroschmeltz Werk, Kempten, Germany) were used as the primary starting materials [14]. To investigate the effect of composition, five distinct composite batches were formulated with CaB_6 content systematically varied from 10 to 50 wt.%, as detailed in Table 1.

Table 1

Composition of Al–CaB_6 ceramic composites
***Таблица 1.* Состав керамических композитов Al–CaB_6**

Sample	Al powder (mass %)	CaB_6 powder (mass %)
CA91	90	10
CA82	80	20
CA73	70	30
CA64	60	40
CA55	50	50

The composite was fabricated using a multi-step process. First, approximately 50 g of the aluminum and CaB_6 powder blend was milled for one hour in isopropanol using a roller ball mill to ensure homogeneity and reduce agglomeration. The slurry was then filtered and dried at 100 °C overnight. Subsequently, the dried powder was mixed with 7 wt.% polyvinyl alcohol (PVA) binder to enhance compatibility. The mixture was uniaxially pressed at 20 kN into pellets (≈1 cm diameter) using a Paul-Otto Weber press (Germany). The resulting green compacts were finally sintered in an air atmosphere at 1300 °C for 2 h to promote microstructural development and densification.

Characterization Techniques

The sintered Al–CaB_6 composites were comprehensively characterized to establish critical structure-property relationships. Phase identification and

crystal structure analysis were conducted using X-ray Diffraction (XRD) on a BRUKER D8 ADVANCE diffractometer with Cu $K\alpha_1$ radiation (λ = 0.15406 Å), operated at 40 kV and 40 mA. Scans from 3° to 70° (2θ) at a step size of 0.02° and a speed of 2° min^{-1} were used to identify all crystalline phases, determine lattice parameters, and detect secondary oxides formed during sintering. The microstructure was then examined using a Philips XL30 Scanning Electron Microscope (SEM, Netherlands) to reveal grain morphology, phase distribution, interfacial connectivity, and overall porosity, which are vital for understanding mechanical and electrical property evolution. Furthermore, chemical bonding and the presence of specific molecular units were probed by Fourier Transform Infrared Spectroscopy (FTIR) on a JASCO FT/IR-6100 spectrometer. The FTIR spectra, collected from 400–4000 cm^{-1} with a 4 cm^{-1} resolution, were essential for confirming the integrity of the fundamental B_6 octahedra within the CaB_6 structure and for identifying surface functional groups and oxide species that could influence dielectric behavior.

The density of the sintered samples was determined using Archimedes' method with distilled water as the immersion medium. The density (ρ) was calculated using:

$$\rho = m\_air / (m\_air - m\_liquid)$$

where m_air is the mass of the dry sample in air and m_liquid is the apparent mass of the sample when immersed in liquid.

RESULTS AND DISCUSSION

X-ray diffraction Analysis

XRD analysis (Fig. 1) of samples sintered at 1300 °C identified multiple crystalline phases, including corundum (α-Al_2O_3), various aluminum borates, calcium aluminum borate, and calcium aluminate. A gradual reduction in CaB_6 peak intensity confirmed its partial decomposition, attributed to a solid–liquid reaction between molten aluminum and CaB_6:

$$3CaB_6 + 14Al \rightarrow 3CaAl_4 + 2AlB_2 + 14B \quad (2)$$

The identification of aluminum diboride (AlB_2) and calcium aluminide ($CaAl_x$) phases confirms this reaction pathway (equation 2). In composites with low CaB_6 content (**CA91–CA64**), corundum and an aluminum borate phase ($Al_{4.8}O_{1.04}$) were predominant, indicating aluminum oxidation during sintering. In contrast, the equimolar composite (**CA55**) exhibited a complex mixture of phases, including aluminum borate ($Al_4B_2O_9$), calcium aluminum borate ($AlBCaO_4$), and calcium aluminate ($CaAl_4O_7$), demonstrating that a balanced Al/CaB_6 ratio promotes extensive interfacial reactions [15]. Consequently, the equimolar Al/CaB_6 composite achieved the highest level of phase evolution and chemical uniformity among all the samples tested.

Sintering pre-compacted Al–CaB_6 powders at 1300 °C for two hours yielded dense, light-grey ceramics, confirming successful consolidation. XRD analysis (Fig. 1) identified multiple crystalline phases, including corundum (α-Al_2O_3, ICDD #96-101-0952), various aluminum borates, calcium aluminum borate, and calcium aluminate, while a gradual reduction in CaB_6 peak intensity confirmed its partial decomposition. This transformation is attributed to a solid–liquid reaction between molten aluminum and CaB_6, (equation 2).

The identification of aluminum diboride (AlB_2) and calcium aluminide ($CaAl_x$) phases in the X-ray diffraction (XRD) patterns serves as direct confirmation of the proposed reaction pathway. The final composition of the material was highly dependent on the initial ratio of aluminum to calcium boride (Al/CaB_6), clearly showing how stoichiometry governs both the speed of the reaction and the nature of the products formed. In composites with a low CaB_6 content (**CA91–CA64**), the material was primarily composed of corundum (α-Al_2O_3) and an aluminum borate phase ($Al_{4.8}O_{1.04}$, ICDD #96-900-5087), indicating that significant oxidation of the aluminum occurred during sintering while the limited amount of CaB_6 remained largely unreacted. In contrast, the equimolar composite (**CA55**) exhibited a far more complex and diverse mixture of phases, including aluminum borate ($Al_4B_2O_9$, ICDD #96-154-1221), calcium aluminum borate ($AlBCaO_4$, ICDD #96-153-9084), and calcium aluminate ($CaAl_4O_7$, ICDD #96-152-7949) [6]. This richness in borate and aluminate compounds demonstrates that a balanced Al/CaB_6 ratio optimally promotes the interfacial reactions necessary to form multiple intermediate compounds. These observations align with the findings of *El-Bassyouni et al.* (2022), who noted that a stoichiometric balance enhances diffusion-driven reactions, leading to complex borate-aluminate structures [15]. Consequently, the equimolar Al/CaB_6 composite achieved the highest level of phase evolution and chemical uniformity among all the samples tested.

Microstructural Analysis

SEM micrographs (Fig. 2) of samples sintered at 1300 °C show dense and refined microstructures. The **CA91** sample, with the least CaB_6, shows a coarse, uneven network of rod-like crystals and isolated nanoclusters. As CaB_6 content increased, nanoparticle aggregation intensified. The **CA55** composite achieved a finely tuned, nanoparticle-dominated architecture. This progressive refinement demonstrates that the

CaB_6 phase acts as an effective microstructural stabilizer, impeding excessive grain growth and promoting stronger interfacial bonding.

Sintering the composites at 1300 °C, as shown in Fig. 2, successfully produced dense and refined microstructures. The process resulted in finely structured grains and a uniform dispersion of cubic calcium boride (CaB_6) particles, with a clear trend of decreasing porosity as the amount of CaB_6 increased [16]. This microstructural evolution was distinctly visible across the different compositions: the **CA91** sample, with the least CaB_6, showed a course, uneven network of rod-like crystals and isolated nanoclusters, pointing to incomplete fusion during sintering. As the CaB_6 content was raised in the **CA82** and **CA73** formulations, the nanoparticles began to aggregate more noticeably, a sign of intensified atomic diffusion and localized rearrangement of particles. The **CA64** composition displayed a significant shift towards maturity, forming well-developed, submicron crystals with very few nano-features, indicating a more uniform and coarsened grain structure. Ultimately, the **CA55** composite with the highest CaB_6 concentration achieved a finely-tuned, nanoparticle-dominated architecture. This progressive refinement, leading to a homogeneous nanostructure in **CA55**, conclusively demonstrates that the CaB_6 phase acts as an effective microstructural stabilizer. It works by impeding excessive grain growth and promoting stronger interfacial bonding throughout the aluminum composite matrix.

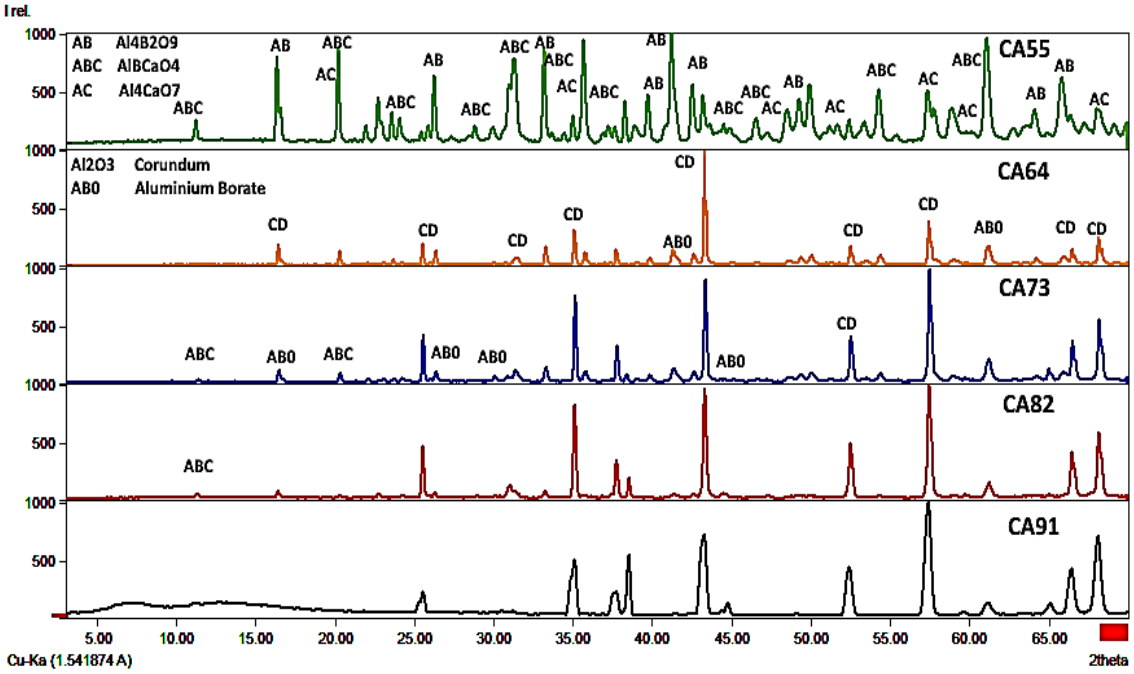

Fig. 1. XRD patterns of the samples sintered at 1300 °C/ 2 h
Рис. 1. Рентгенодифракционные спектры образцов, спеченных при 1300 °C в течение 2 ч

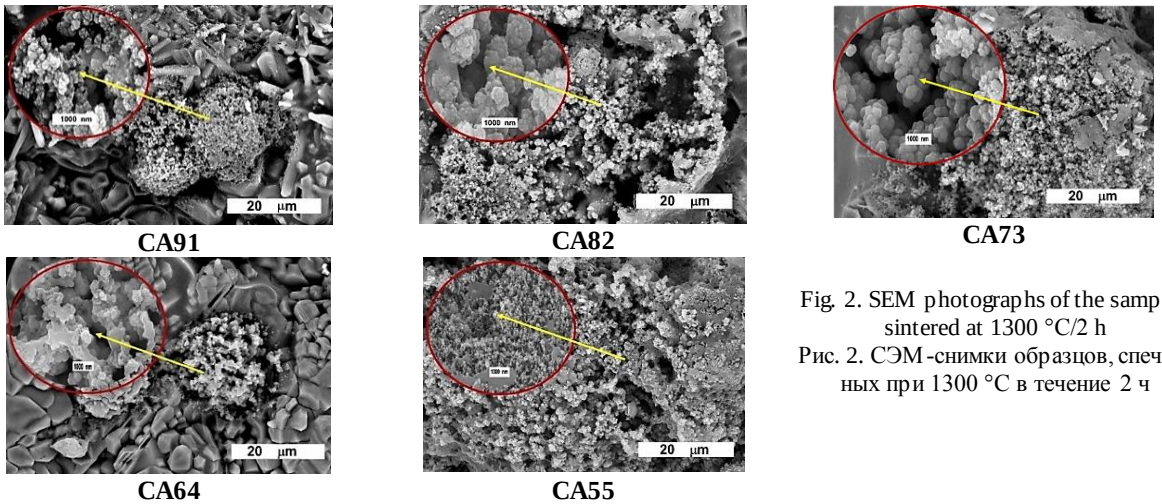

Fig. 2. SEM photographs of the samples sintered at 1300 °C/2 h
Рис. 2. СЭМ-снимки образцов, спеченных при 1300 °C в течение 2 ч

FTIR Analysis

FTIR spectra **(**Fig. 3) provided evidence of chemical bonding and structural changes. The presence of CaB_6 was confirmed by absorption peaks in the 950–700 cm^{-1} range (B_6 octahedral clusters) and below 500 cm^{-1} (B–B stretching). Strong Al–O stretching bands indicated aluminum oxidation, forming Al_2O_3 or Al–O–B interfacial compounds. Detection of B–O–B bending and BO_3 stretching vibrations signifies partial surface oxidation and degradation of CaB_6, leading to borate phases. A detailed peak assignment is provided in Table 2.

The chemical bonding and structural changes within the Al–CaB_6 composites, resulting from the high-temperature 1300 °C sintering process, were effectively revealed by their FTIR spectra (Fig. 3). The analysis identified several distinct absorption bands, which correspond to the specific vibrational energies of the chemical bonds formed in the final material. The presence of the starting CaB_6 phase was clearly confirmed by its unique spectral fingerprints, notably the absorption peaks in the 950–700 cm^{-1} range, which are attributed to the B_6 octahedral clusters, and the peaks below 500 cm^{-1}, associated with direct boron-boron (B–B) stretching vibrations. Simultaneously, the spectra provided direct evidence of oxidation, as strong Al–O stretching bands indicated that part of the aluminum had reacted to form aluminum oxide (Al_2O_3) or other Al–O–B interfacial compounds. Furthermore, the detection of B–O–B bending and BO_3 stretching vibrations signifies that the CaB_6 itself underwent partial surface oxidation and degradation at high temperature, leading to the formation of borate-like or borosilicate phases. Minor, weak absorptions related to O–H and H–O–H bonds were also noted, suggesting a small degree of moisture absorption from the atmosphere after sintering, likely during sample handling or storage. A complete breakdown of all observed absorption bands and their detailed interpretations is systematically presented in Table 2 [17].

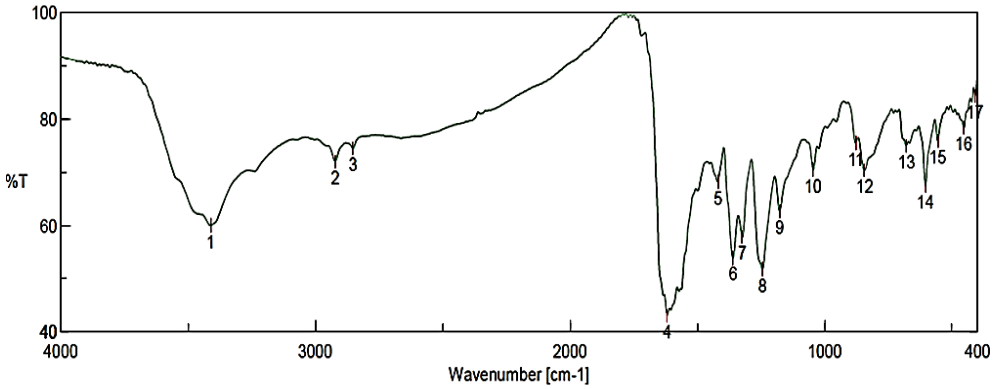

Fig. 3. FTIR of the 70-30 sample sintered at 1300 °C/ 2 h
Рис. 3. ИК-спектр образца 70-30, спеченного при 1300 °C в течение 2 ч

Table 2

FTIR peak assignments and spectral interpretation
***Таблица 2*. Идентификация пиков ИК спектров и интерпретация спектров**

Peak No.	Wavenumber (cm^{-1})	Probable Assignment	Interpretation
1	~3430	O–H stretching	Moisture absorption or residual hydroxyl groups, likely due to surface-adsorbed water or BOH species.
2–3	~2920–2850	C–H stretching (aliphatic)	Possibly from atmospheric hydrocarbon contamination or residual organic species introduced during processing.
4	~1630	H–O–H bending vibration	Indicates adsorbed moisture or water molecules retained in the sample.
5	~1450	B–O asymmetric stretching	Suggests the formation of boron oxide species from partial oxidation of CaB_6 during sintering.
6	~1380	BO_3 stretching	Represents trigonal borate groups formed from oxidation of elemental boron.
7	~1170	B–O–B stretching	Associated with borate glass network formation or oxidized B–O linkages.
8–9	~1100–1000	B–O symmetric stretching	Further confirms the presence of borate networks or degradation products of CaB_6.

Continuation of Table 2

10	~950	Ca–B or B–B modes	Attributed to vibrations of the CaB_6 crystal lattice.
11–12	~870–790	B_6 octahedral stretching	Characteristic of B_6 octahedra in CaB_6, confirming the partial retention of the boride phase.
13	~730	Al–O stretching	Indicates the formation of aluminum oxide due to oxidation of Al during sintering.
14–15	~620–550	Metal–O (Ca–O / Al–O) vibrations	Implies the formation of mixed oxide phases or interfacial reaction products.
16–17	~480–430	B–B stretching in B_6 units	Confirms the presence of intact or partially modified CaB_6 units within the composite.

Table 3

The densities for samples sintered at 1000, 1100, and 1200 °C for 2 h
***Таблица 3.* Плотность образцов, спеченных при 1000, 1100 и 1200 °C в течение 2 ч**

Sample No	1000 °C/ 2 h g/cm^3	1100 °C / 2 h g/cm^3	1200 °C/ 2 h g/cm^3
CA91	2.3768	1.9622	2.1303
CA82	2.3997	2.2595	2.4229
CA73	2.1623	1.9977	2.1858
CA64	2.0414	2.0123	2.0612
CA55	2.1102	2.0012	2.0974

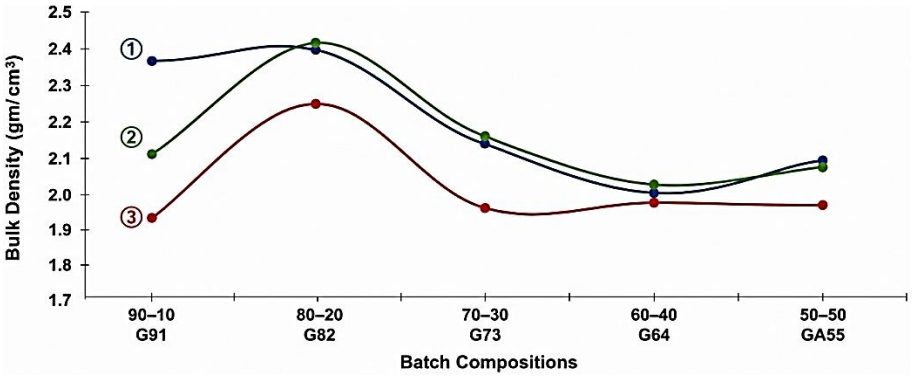

Fig. 4. Densities of the sintered samples at 1000, 1100 and 1200 °C, 1 - 1000 °C, 2 - 1200 °C, 3- 1100 °C. Transcript (gm/cm^3): 1- [2.38, 2.40, 2.17, 2.06, 2.11]; 2- [2.12, 2.43, 2.18, 2.06, 2.10]; 3- [1.95, 2.25, 1.99, 2.02, 2.00] for **G91** (90-10), **G82** (80-20), **G73** (70-30**), G64** (60-40), **GA55** (50-50), respectively

Рис. 4. Плотность спеченных образцов (г/см^3) при 1000, 1100 и 1200 °C, 1 - 1000 °C, 2 - 1200 °C, 3 - 1100 °C :1 - [2,38, 2,40, 2,17, 2,06, 2,11]; 2 - [2,12, 2,43, 2,18, 2,06, 2,10]; 3 - [1,95, 2,25, 1,99, 2,02, 2,00] для **G91** (90-10), **G82** (80-20), **G73** (70-30), **G64** (60-40), **GA55** (50-50) соответственно

The analytical evidence unveils a striking duality within the CaB_6 system: while the particle cores remain faithfully anchored to their original hexagonal framework, the surfaces undergo a dramatic high-temperature metamorphosis. Driven by partial oxidation and chemical interplay with the aluminum matrix, this transformation forges a sophisticated, *in-situ* multiphase boundary composed of borates, calcium aluminates, and mixed oxides. Far from mere byproducts, these secondary phases emerge as the true microstructural "engine," orchestrating the final architecture of primary CaB_6 grains, a reinforcing Al_2O_3 network, and interfacial B_2O_3 layers. In doing so, they exert decisive control over the macroscopic dielectric properties, revealing a reaction mechanism that is as elegantly complex as it is functionally powerful.

Densification Behavior

The measured densities reveal a distinct dependence on both sintering temperature and batch composition. Across all samples, the densities range between 1.96 and 2.42 g/cm^3, showing a clear trend of: a. Increasing density with higher firing temperature (especially up to 1200 °C) and b. Decreasing density with higher CaB_6 content Table 3.

This behavior reflects the complex interplay between metallic Al densification, ceramic phase rigidity, and pore evolution during sintering.

The sintering temperature significantly influenced the densification behavior of the samples, revealing a distinct three-stage process:

- At 1000 °C, moderate densification was achieved (2.04–2.40 g/cm^3), characteristic of solid-

state sintering mechanisms. Sample **CA82** (80% Al / 20% CaB_6) attained the highest density (2.40 g/cm^3), a result attributed to the plastic flow of aluminum filling pores between CaB_6 grains. In contrast, the lower densities of CaB_6-rich compositions (**CA73–CA55**) suggest incomplete particle bonding and significant residual porosity.

- At the transitional temperature of 1100 °C, a notable density drop occurred across all compositions (1.96–2.26 g/cm^3). This anomaly is likely due to partial melting of the aluminum phase, which occurs before sufficient diffusion-driven densification can be achieved. This state may promote detrimental effects such as pore swelling from entrapped gases and microcracking from thermal expansion mismatch, collectively hindering densification and defining 1100 °C as a suboptimal sintering window.
- At 1200 °C, densities recovered substantially (2.06–2.42 g/cm^3), indicating the activation of efficient liquid-phase sintering. Sample **CA82** again achieved the highest density (2.42 g/cm^3), demonstrating that the now fully molten Al optimally facilitates grain rearrangement, enhances diffusion, and eliminates porosity, resulting in a dense composite microstructure with minimal defects. To clarify, two sequential experimental stages were conducted in this study:

1. Sintering optimization stage:

A preliminary investigation was performed at 1000, 1100, 1200, and 1300 °C to evaluate the densification behavior of the composites. The density data presented in Table 2 correspond to this stage and were used to identify the general densification trend and the temperature range at which significant consolidation occurs.

2. Final processing and characterization stage:

Based on the overall densification behavior and the need to ensure complete reaction and microstructural development, all samples selected for detailed characterization (XRD, SEM, FTIR, and dielectric measurements) were sintered at 1300 °C for 2 h. The reference to 1200 °C as an "optimal" temperature in the original manuscript was not intended to indicate that the final characterized samples were processed at this temperature, but rather that it represents a key transition point in densification behavior.

As correctly noted, aluminum melts at approximately 660 °C, and therefore, at the sintering temperatures used in this study (1000–1300 °C), aluminum exists in the liquid state. Under these conditions, densification is governed primarily by liquid-phase-assisted sintering (LPS) rather than purely solid-state diffusion.

Liquid-phase sintering is well established as a mechanism in metal–ceramic systems where a low-melting metallic phase enhances densification through particle rearrangement, capillary forces, and accelerated mass transport [18]. In such systems, the presence of a transient liquid phase significantly improves interparticle contact and promotes rapid densification compared to conventional solid-state sintering.

In the present Al–CaB_6 system, molten aluminum plays a critical role by:

- enhancing particle rearrangement and pore elimination via capillary-driven forces,
- facilitating solid–liquid interfacial reactions with CaB_6, and
- accelerating diffusion processes, leading to the formation of boride and aluminate phases.

This interpretation is consistent with prior studies on aluminum-based composites, where molten aluminum has been shown to promote densification and interfacial reactions during sintering [19]. Similarly, investigations on CaB_6-reinforced aluminum systems confirm that solid–liquid reactions dominate phase evolution and microstructural development at elevated temperatures [20].

Dielectric Studies

The dielectric properties of ceramic composites such as permittivity and loss are critical because they determine how the material responds to electric fields. This directly impacts their performance in key applications like electronics, energy storage capacitors, and high-temperature aerospace systems, making the tailoring of these properties essential for advanced materials engineering [21]. The unique combination of inherently conductive metallic aluminum and the refractory ceramic calcium hexaboride (CaB_6) in the Al/CaB_6 composites creates a highly versatile platform for engineering specific electrical and dielectric responses. This synergy arises from the ability to precisely control the material's composition and microstructure for instance the particle size, distribution, and interfacial phases, which directly governs the balance between conductive pathways and insulating barriers. By manipulating these parameters, one can finely tune the composite's overall behavior, adjusting its charge transport mechanisms and polarization characteristics to suit distinct functional requirements. Therefore, a deep investigation into the dielectric properties of these composites is doubly valuable: it provides critical data for the practical design of components like capacitors, advanced insulators, and high-frequency devices, while also yielding fundamental insights into the core physical phenomena of charge dynamics. This includes understanding polarization mechanisms, dielectric relaxation processes, and the complex movement of electrical charges across the interfaces within this sophisticated heterogeneous architecture [22].

A detailed analysis of the dielectric response in Al/CaB_6 composites across a range of frequencies and material compositions, as illustrated in Fig. 5 through 7, provides critical insight into how interfacial phenomena at the boundaries between aluminum, calcium boride, and the formed oxide phases are the primary governing factors for key electrical parameters. These interfaces directly control the magnitude of the dielectric constant (ε_r) by acting as sites for charge accumulation, influence the energy dissipation measured as dielectric loss (tan δ), and dictate the pathways for electrical conduction under alternating current, known as AC conductivity ($\sigma_a c$). This investigation clarifies the fundamental electrical mechanisms at play, most notably interfacial (Maxwell-Wagner-Sillars) polarization, where charges build up at the internal phase boundaries, as well as space-charge accumulation and subsequent relaxation processes. By understanding these mechanisms, we can identify effective strategies for performance enhancement, such as refining the composite's microstructure to create more uniform phase distributions and optimizing the composition to control interfacial density. Such knowledge is indispensable for advancing the field of functional ceramics, particularly for demanding applications in high-frequency electronics where signal integrity is paramount, in energy storage systems like capacitors that require high polarization with minimal loss, and in thermal management technologies where stable dielectric properties under thermal stress are non-negotiable.

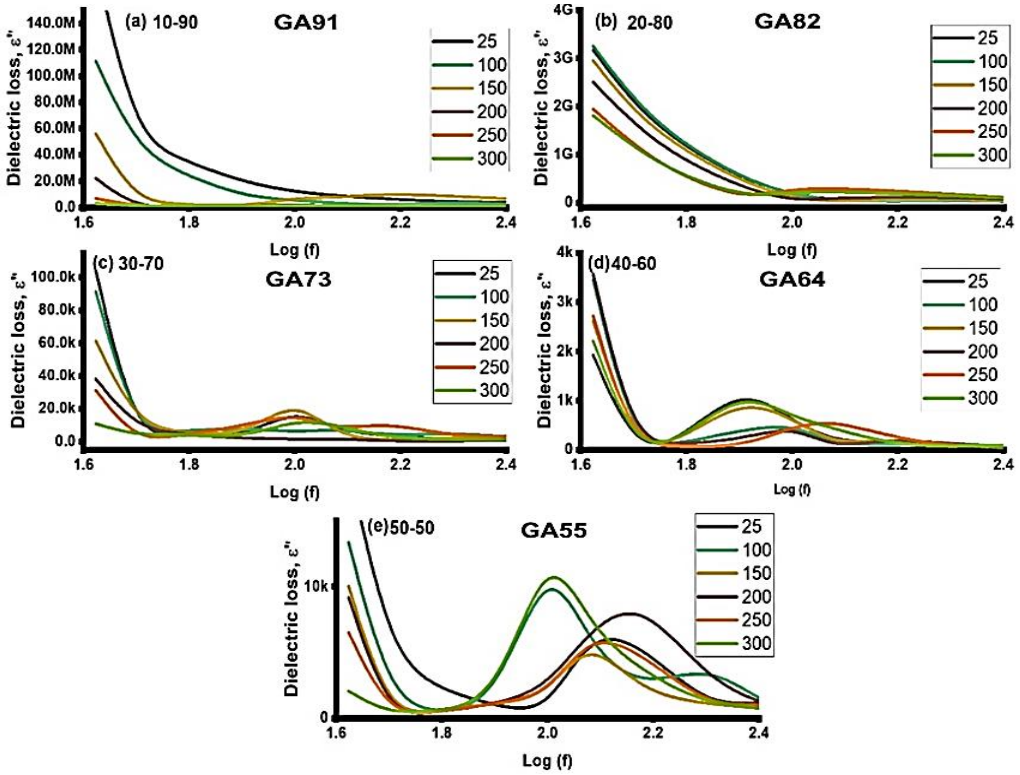

Fig. 5. Frequency dependence of dielectric loss for Al-CaB_6 ceramic composites with varying CaB_6 content, illustrating interfacial polarization effects and relaxation dynamics across the frequency spectrum

Рис. 5. Частотная зависимость диэлектрических потерь для керамических композитов Al-CaB_6 с различным содержанием CaB_6, иллюстрирующая эффекты межфазной поляризации и динамику релаксации в частотном спектре

Dielectric Response and Relaxation Behavior

At low frequencies, every Al–CaB_6 composite showed a significant rise in dielectric loss, an effect that was most extreme in samples containing less CaB_6. This phenomenon is best explained by the Maxwell-Wagner-Sillars (MWS) effect, a type of interfacial polarization that is common in mixed materials like these, which combine conductive aluminum with insulating CaB_6 particles. The stark difference in electrical properties between these two phases causes electric charges to build up and get trapped at their boundaries, much like a traffic jam at a border between two different regions. This localized charge accumulation creates a strong but lagging polarization, which manifests as the high dielectric loss observed at low frequencies [23].

The presence of interfacial oxide layers, particularly aluminum oxide (Al_2O_3) that forms during the high-temperature sintering process, intensifies this energy loss. These oxides act as charge-trapping sites,

hindering the movement of electrical carriers. This restriction leads to a greater buildup of space charge and, consequently, higher energy dissipation as heat. The FTIR analysis provides direct chemical evidence for this, showing clear signatures of Al–O and B–O bonds that confirm the oxidation of aluminum and partial degradation of the CaB_6 surfaces. This direct link between the chemistry at the interfaces and the measured dielectric behavior highlights how critical oxide-matrix interactions are in shaping the composite's overall electrical properties. In contrast, as the CaB_6 content was increased, both the dielectric constant (ε_r) and electrical conductivity showed a steady improvement. This positive trend is attributed to the inherent polarization of the CaB_6 phase itself, whose rigid boron (B_6) octahedral structures contribute strongly to the material's ability to store electrical energy. The material's energy loss (dielectric loss) decreased at lower frequencies for two main reasons: a more uniform structure that blocked errant electrical leaks, and the formation of efficient charge pathways that reduced waste. At higher frequencies, the loss continued to drop because the internal charges could no longer keep up with the rapid changes in the electrical field. Furthermore, the material's energy relaxation was spread over a wide range of frequencies, which is a direct signature of its complex and varied internal structure [24].

The electric modulus analysis provides further evidence for our conclusions. The main clue is that the peaks in the data become broader as more CaB_6 is added [25]. This broadening tells us that the electrical charges within the material can no longer all move in sync; instead, they follow a much wider variety of paths and timelines, a behavior known as Distributed Relaxation Times (DRT). The physical reason for this could be noted in the SEM images (Fig. 2), which show that the fine CaB_6 particles are spread evenly throughout the aluminum, creating a very uniform and dense structure. This specific microstructure controls the electrical properties in three key ways:

1. Maximized Interfaces: By making the CaB_6 grains smaller and spreading them out, we create a huge amount of internal surface area between the two materials. These interfaces are hotspots for polarization (charge build-up), which strengthens the material's ability to store electrical energy, while also allowing us to finely tune how much energy is lost as heat.

2. Oxide Layer Control: The oxides that form at these interfaces act as traffic controllers for electrical charges. Very thin or broken oxide layers (under 5 nm) act like shortcuts, allowing charges to quickly "tunnel" through. In contrast, thicker, continuous oxide layers (over 10 nm) act like roadblocks, trapping charges and slowing them down, which directly shapes how the material relaxes.

3. Manufacturing is Key: The final electrical behavior is not accidental. The sintering conditions (temperature and time) are the primary controls that determine the size of the CaB_6 grains, the thickness of the oxide layers, and the ultimate dielectric performance of the composite [26].

For use in modern electronics and energy storage, a material must have very low energy loss (low dielectric loss) at high frequencies. Our Al-CaB_6 composite achieves this effectively.

We found that adding more CaB_6 increases the material's ability to store electrical charge (dielectric constant) and its conductivity. Crucially, it also ensures a stable performance across a wide range of frequencies. This is because the electrical charges inside the material relax at many different speeds (a "non-Debye" process), so the properties don't change drastically at a single frequency [27]. The energy loss of the material varies significantly with frequency due to different governing mechanisms. At low frequencies, energy loss is high, primarily caused by interfacial polarization, where electrical charges accumulate at the boundaries between the aluminum and CaB_6 phases. At high frequencies, however, this energy loss diminishes. The material's complex microstructure prevents large-scale charge movement, effectively trapping the energy within the structure rather than dissipating it as heat.

In summary, increasing the CaB_6 content successfully creates a composite material that combines a high charge-storage capacity (permittivity) with minimal energy loss at high frequencies. This unique combination of properties makes it an excellent candidate for advanced capacitors and high-frequency electronics.

Frequency Dependence of Dielectric Constant (ε_r)

Fig. 6 shows how the charge-storage capacity (dielectric constant, ε_r) of the Al-CaB_6 composite changes with frequency for different amounts of CaB_6. The key finding is that adding more CaB_6 significantly increases the material's ability to store charge at low frequencies. This happens because the conductive aluminum and insulating CaB_6 grains create countless tiny interfaces. At low frequencies, electrical charges build up at these interfaces, like a traffic jam of charges, which greatly boosts the storage capacity. More CaB_6 means more of these interfaces, leading to even higher storage. However, as the frequency increases past about 1 kHz, the charge-storage capacity drops sharply for all compositions. This is because the electrical field changes too quickly for the charges at the interfaces to keep up, so they can no longer contribute to storage.

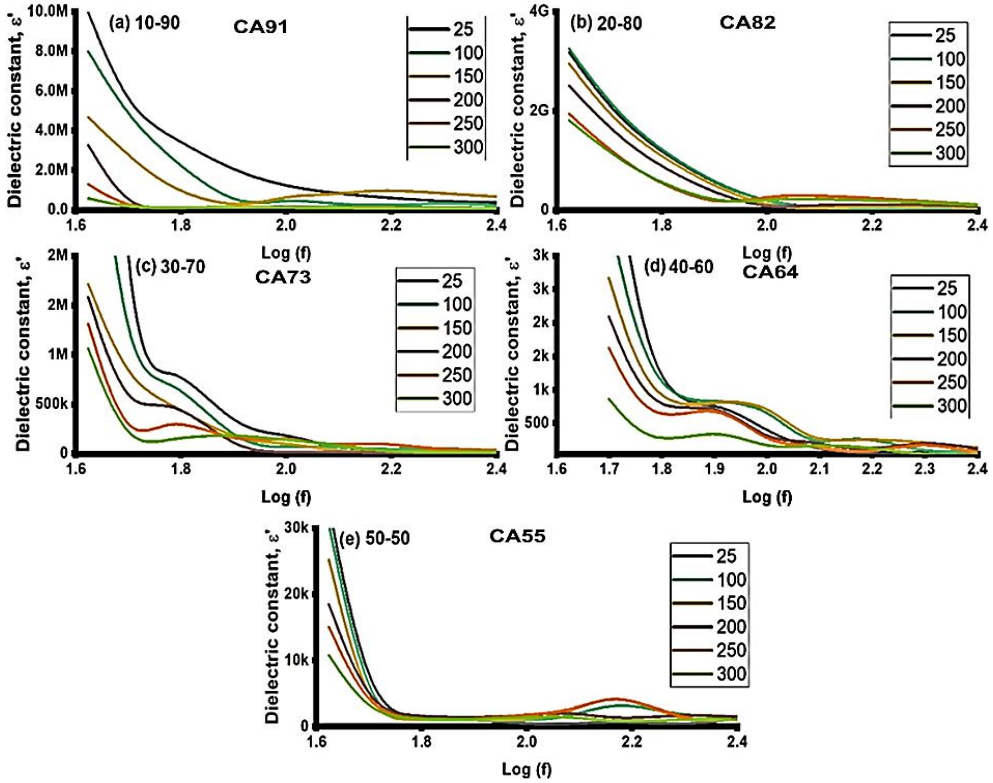

Fig. 6. Variation of dielectric constant (ε') as a function of frequency for Al-CaB_6 composites with different compositions, highlighting the influence of CaB_6 content on low-frequency polarization and dielectric storage capability

Рис. 6. Изменение диэлектрической постоянной (ε') в зависимости от частоты для композитов Al-CaB_6 различного состава, демонстрирующее влияние содержания CaB_6 на низкочастотную поляризацию и диэлектрическую способность

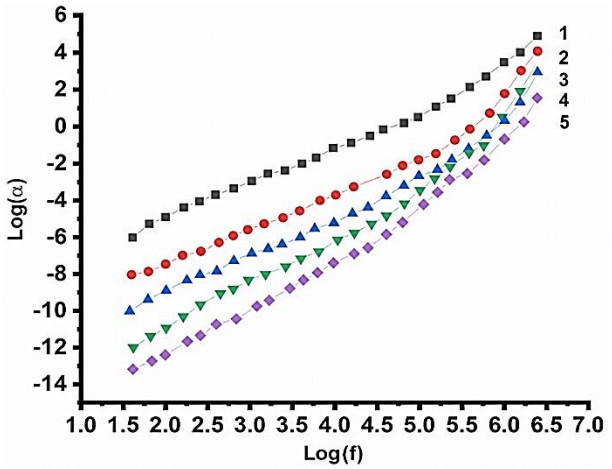

Fig. 7. Log(α) vs Log(f) for different age ranges. 1: **CA91** (10-90); 2: **CA82** (20-80); 3: **CA73** (30-70); 4: **CA64** (40-60); 5: **CA55** (50-50)

Рис. 7. Log(α) против Log(f) для разных возрастных диапазонов. 1: **CA91** (10-90); 2: **CA82** (20-80); 3: **CA73** (30-70); 4: **CA64** (40-60); 5: **CA55** (50-50)

Ultimately, composites with more CaB_6 maintain a higher charge-storage capacity across the entire frequency range measured, demonstrating their effectiveness. The improved ability to store electrical charge (high dielectric constant) stems from two effects that work powerfully together:

1. Intrinsic Molecular Polarization: The CaB_6 additive itself is made of highly polarizable B_6 octahedra. Think of these as tiny, strong molecular magnets that can easily align with an electric field. This inherent property directly boosts the composite's overall charge storage capacity.

2. Enhanced Network Effects: At higher concentrations, the CaB_6 particles get close enough to form connected chains, or "percolative networks," throughout the aluminum. This does two things: it creates a massive amount of internal surface area, which intensifies the charge build-up (interfacial polarization) at the boundaries between materials, and it provides pathways for charges to move and redistribute efficiently across the entire material.

This explanation is grounded in direct physical evidence. The superior performance of High-CaB_6 compositions is confirmed by the SEM images, which show a fine, uniform structure, and by FTIR data, which identified the presence of interfacial oxides.

AC Conductivity Behavior

Fig. 7 reveals the dynamic electrical character of the Al–CaB_6 composites, where the AC conductivity unfolds a clear narrative of charge transport mechanisms across different frequencies. The data adheres

to Jonscher's universal power law, a signature of disordered materials, and reflects the fundamental interplay between the conductive aluminum matrix and the insulating CaB_6 phase [28, 29, 30].

At low frequencies, the conductivity forms a stable "plateau," representing the DC conductivity. Here, in composites with lower CaB_6 content, electrical current flows freely through continuous, highway-like metallic pathways within the aluminum network. As the frequency increases, a pivotal transition occurs: the conductivity begins to rise, following a sub-linear power-law trend. This marks a shift from long-range metallic flow to short-range hopping conduction. In this regime, charge carriers become trapped and must make activated jumps across barriers such as interfaces between grains, thin oxide layers, or isolated metallic islands. The higher the frequency, the more these trapped charges are energized to hop, leading to the characteristic increase in AC conductivity [31]. The composition of the composite acts as a master tuning knob for this behavior. With low CaB_6 content**,** the robust aluminum network ensures high DC conductivity, with the dispersive, hopping-dominated region only appearing at very high frequencies. In contrast, high CaB_6 content disrupts the metallic pathways, fracturing them into isolated islands. This significantly reduces the DC conductivity and causes the dispersive region to emerge at much lower frequencies with a steeper slope. This indicates that interfacial polarization and charge hopping become the dominant conduction mechanisms, as electrons must tunnel through insulating barriers [32, 33].

In summary, by simply varying the CaB_6 fraction, we can systematically engineer a transition in the fundamental conduction mechanism from a metallic, network-driven transport to a defect-activated, hopping-dominated regime. This provides a powerful and versatile strategy for tailoring the electrical properties of Al–CaB_6 composites, directly linking their microscopic architecture to macroscale performance for targeted applications.

CONCLUSION

This study demonstrates that Al–CaB_6 composites are tunable, high-performance materials. The optimal 80% Al - 20% CaB_6 composition, sintered at 1200 °C, achieves a dense, homogeneous microstructure with minimal porosity. This structure arises from a preserved CaB_6 core surrounded by stable interfacial oxides, leading to superior dielectric properties: high charge-storage capacity coupled with low energy loss, driven by optimized interfacial polarization and efficient charge transport.

The densification process is temperature-sensitive, with a temporary density drop at 1100 °C revealing an unstable sintering transition, later resolved at 1200 °C. The synergy of excellent dielectric performance, thermal stability, and mechanical robustness makes these composites ideal for high-frequency electronics, compact energy storage, and thermal management systems. Future work should focus on interfacial engineering and scalable synthesis to enable practical device integration.

ACKNOWLEDGMENTS

This research did not receive any specific grant from funding agencies in the public, commercial, or not-for-profit sectors.

CONFLICT OF INTEREST

The authors declare the absence of a conflict of interest warranting disclosure in this article.

Авторы заявляют об отсутствии конфликта интересов, требующего раскрытия в данной статье.

REFERENCES
ЛИТЕРАТУРА

1. **Ding J., Cui C., Sun Y., Ding J., Zhao L., Cui S.** Microstructures and mechanical properties of in-situ CaB_6 ceramic particles reinforced Al-Cu-Mn composite. *Ceram. Int.* 2019. V. 45. N 17. Pt. A. P. 21668-21675. DOI: 10.1016/j.ceramint.2019.07.165.
2. **Liu J., Cui X., Liu H., Wang Y., Liu S., Wang J., Li X., Xu W., Wang Y., Li H., Cui H., Feng R., Pan Y.** Preparation of CaB_6-Reinforced Al/Al-Si Composites and Study of the Comprehensive Properties. *Int. J. Metal. Casting.* 2024. V. 19. P. 989–998. DOI: 10.1007/s40962-024-01361-1.
3. **Kenawy S.H.** Synthesis Aluminum Borate Ceramic. Proceeding of the 14th Applied Mechanics and Mechanical Engineering (AMME) Conference. 2010. 25-27. DOI: 10.21608/amme.2010.37703.
4. **Karadimas G., Salonitis K.** Ceramic Matrix Composites for Aero Engine Applications-A Review. *Appl. Sci.* 2023. V. 13. N 5. P. 3017. DOI: 10.3390/app13053017.
5. **Smart L.E., Moore E.A.** Solid State Chemistry: An Introduction. 2012. 138 p.
6. **Cui X., Wu Y., Zhu X., Liu X.** In-situ formation of Al-CaB_6 composites with low resistivity. *Rare Metals*. 2012. V. 31. N 6. P. 578. DOI: 10.1007/s12598-012-0561-0.
7. **Khan M.M.** Chemical vapor deposition synthesis method. Chapter 8. In: Photocatalysts: Synthesis and Characterization Methods. 2025. Elsevier. P. 79-89. DOI: 10.1016/B978-0-443-28913-2.00009-5.
8. **Costa L.M., Costa de Souza T.C., Gonçalves de Oliveira R.K.F., Almeida N.G.S., Houmard M.** Effects of silicas and aluminosilicate synthesized by sol-gel process on the structural properties of metakaolin-based geopolymers. *Appl. Clay Sci.* 2025. V. 267. P. 107743. DOI: 10.1016/j.clay.2025.107743.
9. **Cahill J.T., Graeve O.A.** Hexaborides: a review of structure, synthesis and processing. *J. Mater. Res. Technol.* 2019. V. 8. N 6. P. 6321-6335. DOI: 10.1016/j.jmrt.2019.09.041.
10. **Mair P., Goettgens V.S., Rainer T., Weinberger N., Letofsky-Papst I., Mitsche S., Leichtfried G.** Laser powder bed fusion of

nano-CaB_6 decorated 2024 aluminum alloy. *J. Alloys Compd.* 2021. V. 863. P. 158714. DOI: 10.1016/j.jallcom.2021.158714.
11. **Ouhassan Y., Bri S., El Boubakraoui M.C., Habibi M.** Dielectric properties of ceramic composite materials based on alumina reinforced by titanium carbide. *FME Transact.* 2020. V. V. 8. N 4. P. 908-913. DOI: 10.5937/fme2004908O.
12. **Lunn K.F., Apelian D.** Thermal and Electrical Conductivity of Aluminum Alloys: Fundamentals, structure-property relationships, and pathways to enhance conductivity. *Mater. Sci. Eng. A.* 2024. V. 924(2972). P. 147766. DOI: 10.1016/j.msea.2024.147766.
13. **Faouzia T., Teixeira S.S., Graca M.P.F., Iben Nassar K.** A Comprehensive Review of Recent Advances in Perovskite Materials: Electrical, Dielectric, and Magnetic Properties. *Inorganics.* 2025. V. 13. N 3. P. 67. DOI: 10.3390/inorganics13030067.
14. **El‐Bassyouni G.T., ElShebiney S., Korany R., Mabrouk M., Soliman A., Darwish H., Kenawy S., Hamzawy E.M.A.** Engineered Calcium Silicate‐Hexaboride Biocomposites: A Versatile Platform for Personalized Orthopedic Therapies. *Silicon.* 2025. V. 17. P. 873–887. DOI: 10.1007/s12633-025-03229-3.
15. **El-Bassyouni G.T., El-Rafei A.M., Azooz M.A., Kenawy S.H., Darwish H., Hamzawy E.M.A.** Preparation, Characterization and biocompatibility of Nominal Wollastonite/Calcium Hexaboride composites. *Mater. Chem. Phys.* 2022. V. 289. P. 126337. DOI: 10.1016/j.matchemphys.2022.126337.
16. **Zhang J., Lei S., An X., Xu X., Chen B., Li H., Yao W., Wang Q., Kong Q.** Effect of CaB6 addition on the microstructure and mechanical properties of Ti-24Nb-4Zr-2.5Mn alloys fabricated by spark plasma sintering. *J. Mater. Res. Technol.* 2024. 30. P. 2264-2271. DOI: 10.1016/j.jmrt.2024.04.214.
17. **Tsebulya G.G., Kozina G.K., Zakharchuk A.P., Kovalev A.V., Dudnik E.M.** Investigation of infrared spectra and determination of the main optical constants of CaB_6. *Powder Metal.Metal Ceram.* 1997. V. 36. N 7-8. P. 413-415. DOI: 10.1007/BF02676003.
18. **Zhou J., Duszczyk J.** Liquid phase sintering of an AA2014-based composite prepared from an elemental powder mixture. *J. Mat. Sci.* 1999. V. 34. P. 545 – 550. DOI: 10.1023/A:1004594628862.
19. **Barry Carter C., Grant Norton M.** Ceramics materials. Science and engineering. Springer science + Business Media, LLC. 2007. 727 p.
20. **Бахаа Абдхади Ахмед, Байдаа К. Аль-Рубайе, Лекаа К. Абдул Карем, Ахмед М. Халил, Сайед Х. Кенави.** Простой синтез и характеризация новых неорганических стеклокерамических композитов для применения в качестве метода замены кости. *Изв. вузов. Химия и хим. технология.* 2026. Т. 69. Вып. 4. С. 67-76. **Bahaa Abdhadi Ahmed, Baidaa K. Al-Rubaye, Lekaa K. Abdul Karem, Ahmed M. Khalil, Sayed H. Kenawy.** Facile synthesis and characterization of novel inorganic glass-ceramic composites for bone replacement applications. *ChemChemTech [Izv. Vyssh. Uchebn. Zaved. Khim. Khim. Tekhnol.].* 2026. V. 69. N 4. P. 67-76. DOI: 10.6060/ivkkt.20266904.6810.
21. **Li D., Zeng X., Li Z., Shen Z.-Y., Hao H., Luo W., Wang X., Song F., Wang Z., Lia Y.** Progress and perspectives in dielectric energy storage ceramics. *J. Adv. Ceram.* 2021. V. 10. N 4. P. 675–703. DOI: 10.1007/s40145-021-0500-3.
22. **Castillo-Robles J.A., Dimas-Muñoz A.P., Rodríguez-García J.A., Calles-Arriaga C.A., Armendáriz-Mireles E.N., Pech-Rodríguez W.J., Rocha-Range E.** Mechanical and Microstructural Response of Aluminum Composites Reinforced with Ceramic Micro-Particles. *J. Compos. Sci.* 2021. V. 5. P. 228. DOI: 10.3390/jcs5090228.
23. **Samet M., Kallel A., Serghei A.** Maxwell-Wagner-Sillars interfacial polarization in dielectric spectra of composite materials: Scaling laws and applications. *J. Compd. Mater.* 2022. V. 56. N 20. P. 3197-3217. DOI: 10.1177/00219983221090629.
24. **Hill R.M., Dissado L.A.** Debye and non-Debye relaxation. *J. Phys. C: Solid State Phys.* 1985. V. 18. N 19. P. 3829. DOI: 10.1088/0022-3719/18/19/021.
25. **Tian F., Ohki Y.** Electric Modulus Powerful Tool for Analyzing Dielectric Behavior. *IEEE Trans. Diel. Electr. Insul.*. 2014. V. 21. N 3. P. 929-931. DOI: 10.1109/TDEI.2014.6832233.
26. **Carter C.B., Norton M.G.** Sintering and Grain Growth. In: Ceramic Materials. 2007. DOI: 10.1007/978-0-387-46271-4_24.
27. **Heikal Sh., El-Bassyouni G.T., Hamzawy E.M.A.** Characterization, Dielectric and AC Electrical Properties of B_2O_3-Al_2O_3-BaO_{-x}-TiO_2 (x = 0, 10, 15, and 20) Thermally Treated Glass. *J. Non-Cryst. Solids.* 2025. V. 666. P. 123687. DOI: 10.1016/j.jnoncrysol.2025.123687.
28. **Popov I.I., Nigmatullin R.R., Khamzin A.A., Lounev I.V.** Conductivity in disordered structures: Verification of the generalized Jonscher's law on experimental data. *J. Phys.: Conf. Ser.* 2012. V. 394. P. 012026. DOI: 10.1088/1742-6596/394/1/012026.
29. **Abd El-Shakour Z.A., El-Bassyouni G.T., Hamzawy E.M.A., Mahdy M.A., El Zawawi I.K., Sherif H.H.A., Turky G.M.** Magnetic and Electrical Properties of Pseudowollastonite Nanoceramic Prepared by Wet Method. *Sci. Rep.* 2025. V. 15. P. 32540. DOI: 10.1038/s41598-025-18717-0.
30. **Ponomarev S.G., Kornyushin M.V., Smirnov A.V., Rybalchenko V.V.** Ceramic Composites of the Calcium Copper Titanate with Giant Dielectric Permittivity. *Russ. J. Gen. Chem.* 2024. V. 94. P. 1537–1539. DOI: 10.1134/S1070363224060331.
31. **Hamzawy E.M.A., El-Bassyouni G.T., Azooz M., Turky G.M.** Electrical Properties of Lithium Silicates Based Glasses and Their Glass-Ceramics. *J. Mater. Sci.: Mater. Electron.* 2024. V. 35. N 3. P. 253. DOI: 10.1007/s10854-024-11981-2.
32. **Gomaa M.M., Kenawy S.H.** Electrical and Physical Properties of Ceramic Whiskers from the Al_2O_3–CaB_6 System. *Interceram.* 2020. V. 69. P. 34–43. DOI: 10.1007/s42411-020-0423-y.
33. **Shchegolkov A., Shchegolkov A., Komarov F.F., Parfimovich I.D., Zemtsova N.V.** Electro- and Thermophysical Properties of Organosilicon Elastomers Modified with Carbon Nanotubes and Microscale Metallic Structures. *Russ. J. Gen. Chem.* 2024. V. 94. N 6. P. 1574-1579. DOI: 10.1134/S1070363224060409.

Поступила в редакцию (Received) 06.04.2026
Принята к опубликованию (Accepted) 29.04.2026